Geophysical Research Letters

RESEARCH LETTER
10.1029/2020GL091331

Key Points:

- Geodynamic models reproduce the high-resolution tomographic images of the Tonga slab
- Collision between a relic and Tonga slabs controls the intense deformation within the two slabs
- Simulated thermal structures predict deep earthquake doublet (*Mw* 8.2 and 7.9) occurs in the warm slab areas

Supporting Information:

Supporting Information may be found in the online version of this article.

Correspondence to:

H. Liu and M. Gurnis,
liuhao@caltech.edu;
gurnis@caltech.edu

Citation:

Liu, H., Gurnis, M., Leng, W., Jia, Z., & Zhan, Z. (2021). Tonga slab morphology and stress variations controlled by a relic slab: Implications for deep earthquakes in the Tonga-Fiji region. *Geophysical Research Letters*, *48*, e2020GL091331. https://doi.org/10.1029/2020GL091331

Received 19 OCT 2020
Accepted 7 MAR 2021

Tonga Slab Morphology and Stress Variations Controlled by a Relic Slab: Implications for Deep Earthquakes in the Tonga-Fiji Region

Hao Liu[1,2,3], Michael Gurnis[3], Wei Leng[1,2], Zhe Jia[3], and Zhongwen Zhan[3]

[1]Laboratory of Seismology and Physics of Earth's Interior, School of Earth and Space Sciences, University of Science and Technology of China, Hefei, China, [2]CAS Center for Excellence in Comparative Planetology, Hefei, China, [3]Seismological Laboratory, California Institute of Technology, Pasadena, CA, USA

Abstract Deep focus earthquakes within the Tonga-Fiji subduction system account for about two-thirds of the global total and provide significant constraints on slab deformation. The factors controlling the intense deformation remain unclear. Here, we use two-dimensional, time-dependent geodynamic models to study the morphology, stress state, and thermal structure of the Tonga-Fiji subduction zone. The results, consistent with tomographic images and focal mechanisms, demonstrate that collision between a relic slab from the Vanuatu Trench and the Tonga slab may control the steeper dip of the Tonga slab and earthquakes in the mantle transition zone. We suggest that the magnitude 8.2 and 7.9 earthquakes in 2018 mostly ruptured within the warm rim of the Tonga slab and occurred beneath the folding relic slab with high temperatures of at least ~900°C and ~1100°C, respectively. The findings support the hypothesis that local slab temperature likely controls rupture of deep earthquakes.

Plain Language Summary Deep earthquakes at the depths between 300 and 700 km are controversial as the increase of temperature and pressure with depth will promote ductile flow and inhibit brittle failure. Approximately two-thirds of the deep earthquakes globally are located below the North Fiji Basin which provides significant constraints on the deformation of the Tonga slab. However, the factors controlling the intense deformation remain unclear. Here, a time-evolving mechanical model is used to study the morphology, state-of-stress, and thermal structure of the Tonga-Fiji subduction zone. The models reproduce the high-resolution Tonga slab morphology and can better fit the focal mechanisms of the deep earthquakes, which demonstrate that collision between a relic slab detached from the Vanuatu Trench and the Tonga slab leads to the nearly vertical Tonga slab and controls the occurrences of the deep earthquakes in the mantle transition zone. We suggest that two large deep earthquakes with moment magnitude (*Mw*) 8.2 and 7.9 in 2018 occurred within the warm rim of the Tonga slab and beneath the high-temperature folded relic slab, respectively, supporting the hypothesis that local slab temperature probably controls the rupture details of deep earthquakes.

1. Introduction

The origin of earthquakes at depths of 300–700 km within sinking cold slabs remains uncertain. Shallow seismic rupture is produced by brittle-frictional processes. However, increasing temperature and pressure with depth promotes ductile flow which inhibits sliding (Houston, 2015; Zhan, 2020). Nevertheless, different mechanisms have been advanced for the nucleation of deep focus earthquakes, including a metastable olivine phase transition in the cold core of a slab (Green & Houston, 1995; Shen & Zhan, 2020; Wiens et al., 1993), thermal instability (Karato et al., 2001; Ogawa, 1987; Ohuchi et al., 2017), and dehydration embrittlement (Barcheck et al., 2012; Hacker et al., 2003; Silver et al., 1995); these mechanisms remain debated (Zhan, 2020).

With rapid subduction of the old Pacific Plate (Figure 1a) beneath the Australian Plate since the Eocene (Müller et al., 2016; Seton et al., 2012), approximately two-thirds of the world's deep earthquakes occur within the Tonga slab (Frohlich, 2006; Gurnis et al., 2000). Global centroid moment tensor (CMT) focal mechanisms show an extensive subhorizontal distribution (~300 km) within the mantle transition zone below North Fiji Basin and with a complex stress state (Alpert et al., 2010; Chen & Brudzinski, 2001; Isacks & Molnar, 1971). For the northern-most slab (north of 21°S), downdip tension is dominant at depths

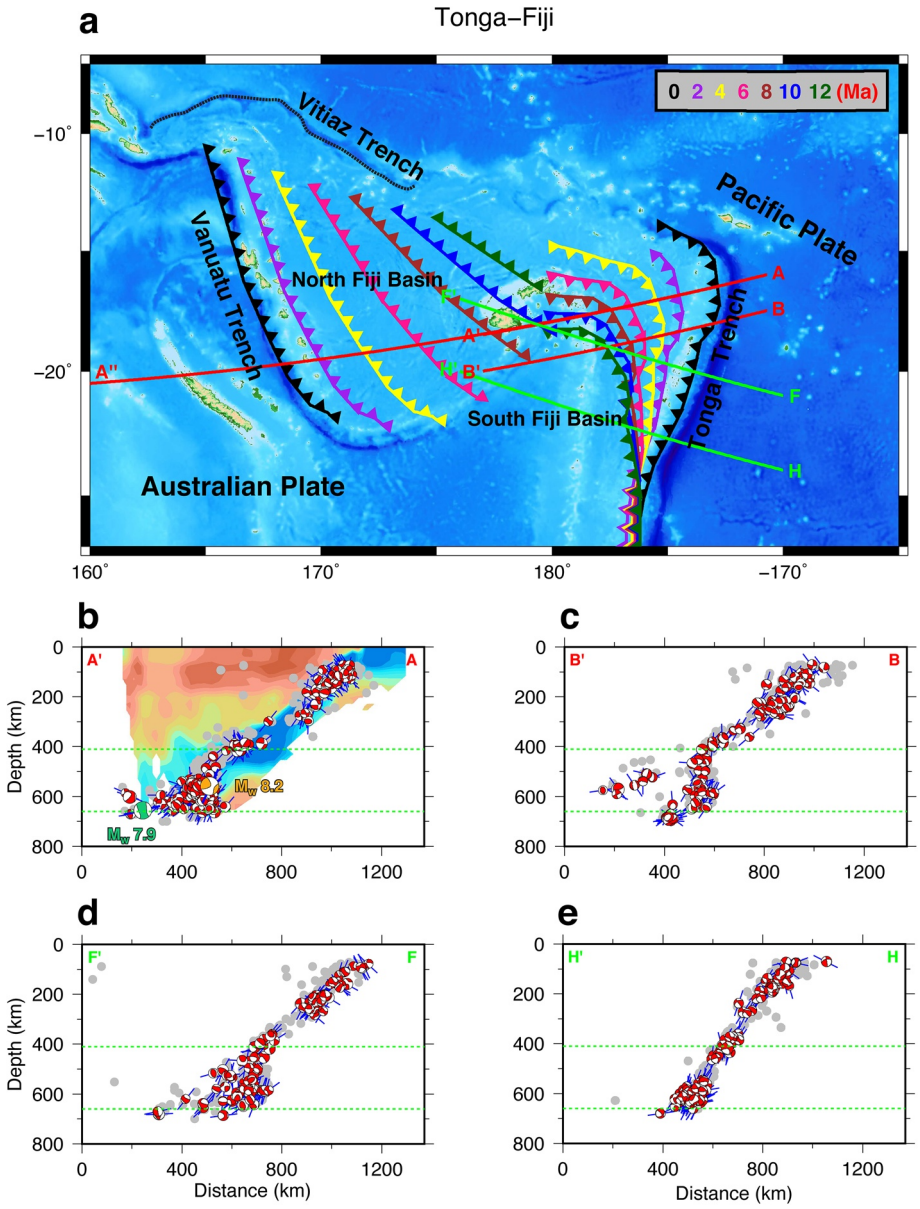

Figure 1. (a) Tectonic setting in the Tonga-Fiji region. Tonga Trench and Vanuatu Trench over past 12 Myr are marked by colored lines (Seton et al., 2012). Black dashed line represents the extinct Vitiaz Trench. Red and green lines are labeled cross sections of seismicity (Table S1), and the A-A″ profile is used to show the Tonga slab morphology from different global *P* wave tomography models displayed in Figure S3. (b–e) Earthquake distributions along the cross-sections in (a). Gray circles represent earthquakes from the ISC-EHB catalog (Engdahl et al., 1998). Beach balls show global centroid moment tensor (CMT) focal mechanisms. Blue lines represent the orientations of the compressional (*P*) axes of the CMT solutions. The green dashed lines represent 410 km and 660 km depths, respectively. We regard the high-resolution tomographic image of the Tonga slab as the background in (b) modified from Conder and Wiens (2006). The 2018 Fiji deep earthquake doublet with *Mw* 8.2 and 7.9 has been projected on the profile.

shallower than 300 km where there may be a double seismic zone with upper layer events showing downdip compression and lower layer events showing downdip tension (Alpert et al., 2010; Bonnardot et al., 2009; Wei et al., 2017). In the mantle transition zone, the averaged stress orientation (*P* axes) is northeast (Alpert et al., 2010). Far outboard of the Tonga Wadati-Benioff zone (WBZ), however, *P* axes are oriented away from the Tonga slab at depths between 500 and 600 km, whereas compressive directions go toward the dipping Tonga WBZ beneath the transition zone (Figures 1b and 1c, Figures S1 and S2). South of 21°S, stress state within the Tonga slab looks simple, being in downdip compression throughout (Figures 1d and 1e;

Bonnardot et al., 2009). Thus, previous studies have suggested that a relic recumbent slab is lying on top of the Tonga slab in the north (Cai & Wiens, 2016; Chen & Brudzinski, 2001; Fan et al., 2019). However, the origin of the remnant slab remains unclear, a relic slab below the North Fiji Basin has been interpreted to be either from the current Tonga slab or an extinct Vitiaz Trench (Cai & Wiens, 2016; Chen & Brudzinski, 2001; Hamburger & Isacks, 1987). More recent analysis of seismicity and tectonic history have interpreted these outboard deep earthquakes as arising from detachment of the Vanuatu slab as the Vanuatu Trench rapidly migrated southwestward accompanied by the formation of the North Fiji Basin over the Miocene (Richards et al., 2011; Seton et al., 2012). Collision of oceanic plateaus west of the Vitiaz Trench at ~12–13 Ma terminated southwest-dipping Vitiaz subduction while initiating northeast-dipping subduction of the Australian Plate along the Vanuatu Trench. Some reconstructions suggest the age of Vanuatu subduction initiation to be 15 Ma (Auzende et al., 1988; Macfarlane et al., 1988; Pelletier et al., 1993). The plate subducting at the Vanuatu Trench should be relatively young having formed by back-arc spreading by Tonga Trench retreat. Tonga subduction initiated near the Norfolk Ridge and New Caledonia at ~50 Ma (Meffre et al., 2012; Sutherland et al., 2017, 2020). Hence, eastward rollback of Tonga starts as early as ~50 Ma with a large South Fiji Basin forming by back arc spreading (Seton et al., 2012). The relic slab is derived from the northern extension of this basin which subducted to the northeast along the Vanuatu Trench. Thus, the oldest possible age of the subducting plate at Vanuatu Trench is ~50 Ma (earliest age of Tonga eastward migration) minus ~12 Ma (youngest age of Vanuatu initiation) or 38 Myr old. However, the subduction plate at the eastern end of the new Vanuatu Trench is likely to be younger, as the plate subduction formed further east after the time of Tonga inception.

Regional and global tomographic imaging shows a complex double-layer morphology of slabs in the transition zone, with the Tonga slab apparently "stagnating" at the top of the lower mantle with large amounts of slab material in the lower mantle beneath the North Fiji Basin (Figure S3; Fukao & Obayashi, 2013; Hall & Spakman, 2002; van der Hilst, 1995). A high-resolution image of the Tonga slab in the upper mantle (Figure S4; Conder & Wiens, 2006) in particular shows that the morphology changes from shallow-dipping just above 500 km to nearly vertical in the lower half of the mantle transition zone, a change in morphology clearly reflected in seismicity (Figure 1 and Figure S2).

The elevated deep earthquakes within Tonga have been attributed to reactivation of slab structures, mantle phase transformations, or resistance imposed by the Pacific superplume (Billen, 2020; Gurnis et al., 2000; Jiao et al., 2000; Kirby et al., 1996), which are related to the thermal structure and state-of-stress of a slab in the transition zone (Green & Houston, 1995; Karato et al., 2001). Recently, a novel observation has shown that a large deep earthquake doublet with *Mw* 8.2 and 7.9 in 2018 occurs in the warmer rim of the Tonga slab and a warm relic slab lying on top of the Tonga slab, respectively. Jia et al. (2020) argued that local temperature in the slab controls the rupture details of deep earthquakes. The inferences are in contrast with traditional interpretation of Tonga, one of the coldest slabs. The new observations and inferences provide a rare opportunity to further investigate the thermal structure, geodynamics, and deformation of deep slabs. Here, we systematically use geodynamic models to better understand the state-of-stress and thermal structure of Tonga and relic slabs, and to better interpret the seismic observations.

2. Method

We model a viscously dominated, incompressible fluid and systematically investigate the influence of a relic slab on the morphology and stress state of the Tonga slab. Details on the constitutive relations, computational method, and boundary conditions are described in the Supporting Information.

The models are formulated to match the known history and kinematics of the region. Recent global plate reconstructions (Müller et al., 2016; Seton et al., 2012; Torsvik et al., 2019) show that the Tonga trench rolled backward ~1,500 km, with average subducting and overriding plates velocities of 8 and 4 cm/yr. Mechanical boundary conditions on the top surface must be imposed, either free-slip with only forces from the local slab or kinematic with the combined influence from the converging Pacific plate and local forces. With the Pacific Plate moving with the sum of the forces around its periphery and with it moving at twice the rate on average since 50 Ma compared to the Australian Plate, kinematic boundary conditions are applied at the surface, while other boundaries are free slip (Christensen, 1996; Han & Gurnis, 1999; Yang et al., 2017).

Nevertheless, the imposed plate motion could influence the state-of-stress and so fully dynamic models (see Supporting Information) are also used. The surface boundary conditions are time-dependent, since Tonga has undergone substantial Cenozoic trench rollback (Seton et al., 2012). Seismic reflection and rock samples from the Tasman Sea demonstrate that there was a period of widespread Eocene plate compression after 53–48 Ma that lasted until at least 37-34 Ma (Sutherland et al., 2017, 2020). This subduction initiation phase is avoided by setting initial trench retreat at 38 Ma. The surface plate motions are prescribed consistent with the regional plate tectonics so that we can control these factors and investigate the influence of the relic slab on Tonga slab morphology and stress distribution within Tonga-Fiji subduction system.

3. Results

We start with a slab in which subducting and overriding plate velocities are 8 and −4 cm/yr, respectively (Case 1, S02.avi, Figures 2a–2d). Time 0 of the forward model is assumed to be 50 Ma for comparison with plate reconstructions (Figure 1). The slab sinks through the upper mantle with high dip due to the large subducting velocity. Buckling and folding occur when the slab reaches the 660 km discontinuity at ~35 Ma, while subsequently descending into the lower mantle. The slab apparently stagnates in the transition zone extending horizontally over ~1,000 km with a low dip, but with a large volume sinking into the lower mantle (S02.avi, Figures 2a–2d). We compute a second model (Case 1_r1) starting at 10 Ma (that is 40 Myr into Case 1) by inserting a relic slab assumed detached from the Vanuatu Trench. The ages of the relic slab change linearly along the slab dip from 35 to 15 Myr (Table S3). After ~2 Myr, the relic slab collides with the Tonga slab. With ongoing Tonga Trench retreat, strong mantle flow flips the relic slab over. Finally, after 10 Myr (0 Ma) of further slab descent, the folded relic slab leans atop the Tonga slab. The Tonga slab is forced downward by the additional negative buoyancy of the relic slab such that the morphology changes from being more horizontal atop the transition zone to nearly vertical in the lower half of the transition zone (S01.avi, Figures 2e–2h). Furthermore, the Tonga slab becomes horizontal toward the west for ~600–700 km at the top of the lower mantle. The interaction between the Tonga and relic slabs reproduces the fine-scale structure of the Tonga slab clearly evident in tomography and seismicity (Figure 1, Figures S2–S4; Conder & Wiens, 2006; van der Hilst, 1995).

The addition of a relic slab descending atop a preexisting slab leads to pronounced differences in the state-of-stress of the initial slab, especially when focusing on the slab in the upper mantle and transition zone (red and green rectangles in Figure 2). We first show evolution of principal compressive stress in the transition zone during relic and Tonga slab collision (Figure 3). At the initial collision stage, the relic slab squeezes and pushes the Tonga slab toward the right and downward leading to nearly vertical compression in the relic and Tonga slabs (Figures 3a–3c). With ongoing squeezing, the state-of-stress within the Tonga slab becomes downdip compression. Meanwhile, the compression directions within the folding relic slab are either away from or rotate toward the steep Tonga slab in the upper and lower part, respectively (Figures 3d–3f). The state-of-stress within the two slabs over all depths at 0 Ma is shown with observed focal mechanisms (Figure 4). Near the cold core of the single Tonga slab model (Case 1), the slab is in downdip compression throughout (Figures 4a and 4b). If a fully dynamic formulation is used (Supporting Information), then slabs can also be in downdip compression throughout (Figure S12). In the model with the relic slab (Case 1_r1), the stress state near the cold core of the slab in the upper mantle shows a transition from downdip compression in the upper part of the slab to downdip tension in the lower part over a scale of ~30 km (Figure 4c). Generally, rigid slabs efficiently transmit stress from the positive buoyancy of the postspinel phase transition and from resistance from the 660 km viscosity contrast to shallow depths. However, most of the Tonga slab is located in the lower mantle which will substantially increase the negative buoyancy; therefore, a double-layered stress pattern occurs. This pattern coincides with focal mechanisms dominated by downdip tension with a double seismic zone above 300 km (Wei et al., 2017). In the transition zone, state-of-stress within the relic slab is more complex due to buckling. At depths between 450 and 600 km, the modeled orientations of compressional stress depart from the Tonga slab in the relic slab's core and are nearly horizontal at the margin, whereas the principal compressive directions rotate toward Tonga slab beneath the transition zone (Figure 4d). It appears to be consistent with the focal mechanisms of the outboard deep earthquakes (Figures 1 and 4d). There are a large number of earthquakes in the transition zone and so following Alpert et al. (2010) we obtain averaged stress orientation between 525 and 575 km based on *P*

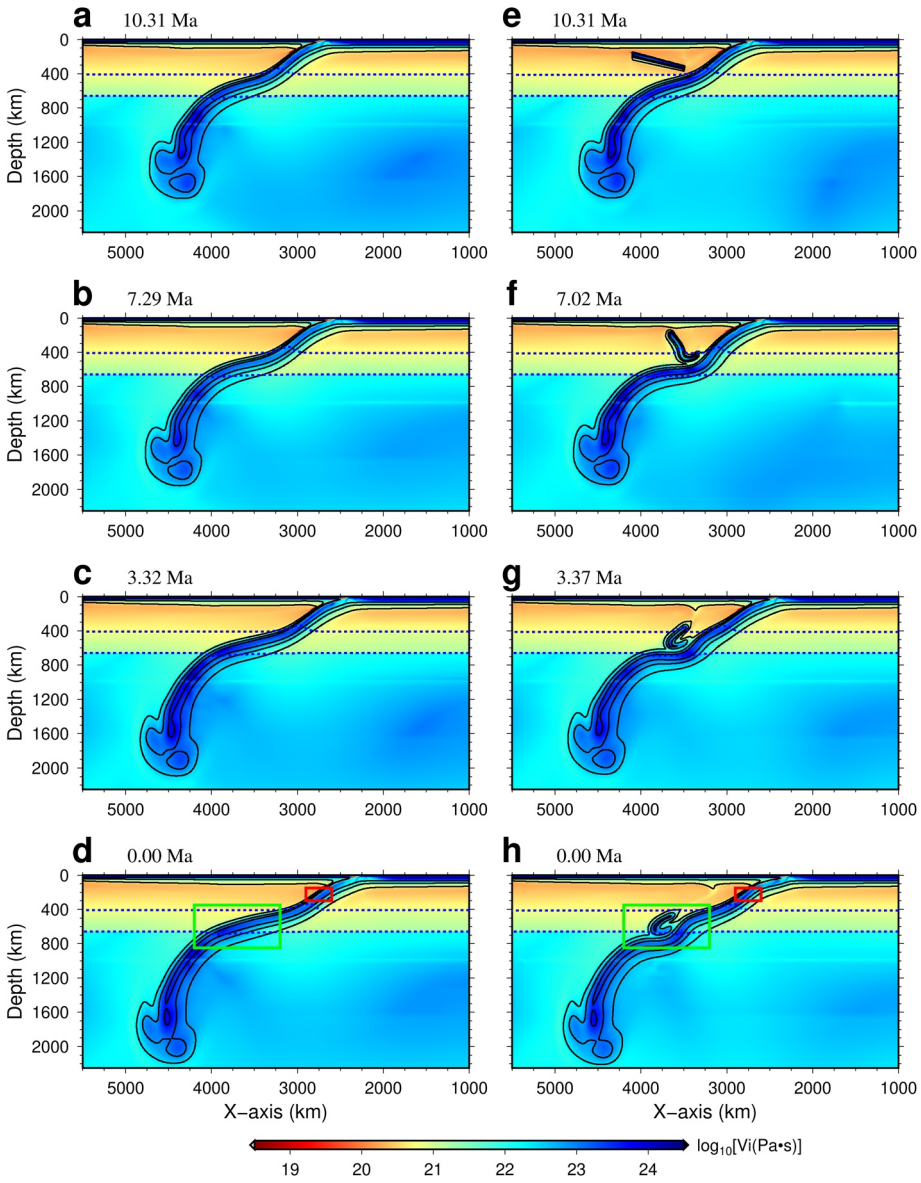

Figure 2. Viscosity field evolution for Case 1 (a–d) and Case 1_r1 (e–h). The black lines show the temperature contours of 800°C, 1050°C, and 1300°C, respectively. The blue dashed lines represent the 410 and 660 km phase transitions. We will zoom in the red and green rectangles to investigate the stress state within slabs later.

axis orientations along the widened A–A′ and B–B′ profiles (Table S1). Computed principal compressional stresses can well fit the averaged stress orientation estimated by focal mechanisms (black line in Figure 4d). There is a seismicity gap between Tonga and relic slabs which we attribute to ductile flow at high temperature within the collisional interface (Figures 1 and 4d). Moreover, the averaged forces along the slab core in the transition zone over the last 5 Myr computed for the single Tonga slab model and Tonga-relic slab model are −109.37 and −78.41 MPa, respectively, which demonstrates that the relic slab decreases the compression in the transition zone, answering why downdip tension occurs in the shallow part of the slab. Thus, the Tonga-relic slab model seems to be capable of explaining the focal mechanisms throughout the northern Tonga subduction zone.

Although there is considerable complexity in the state-of-stress within the main Tonga slab (e.g., the cold core of the slab), the pattern is one of downdip compression throughout without a relic slab. If the relic is added, then the state-of-stress changes within the upper mantle from downdip compression to tension

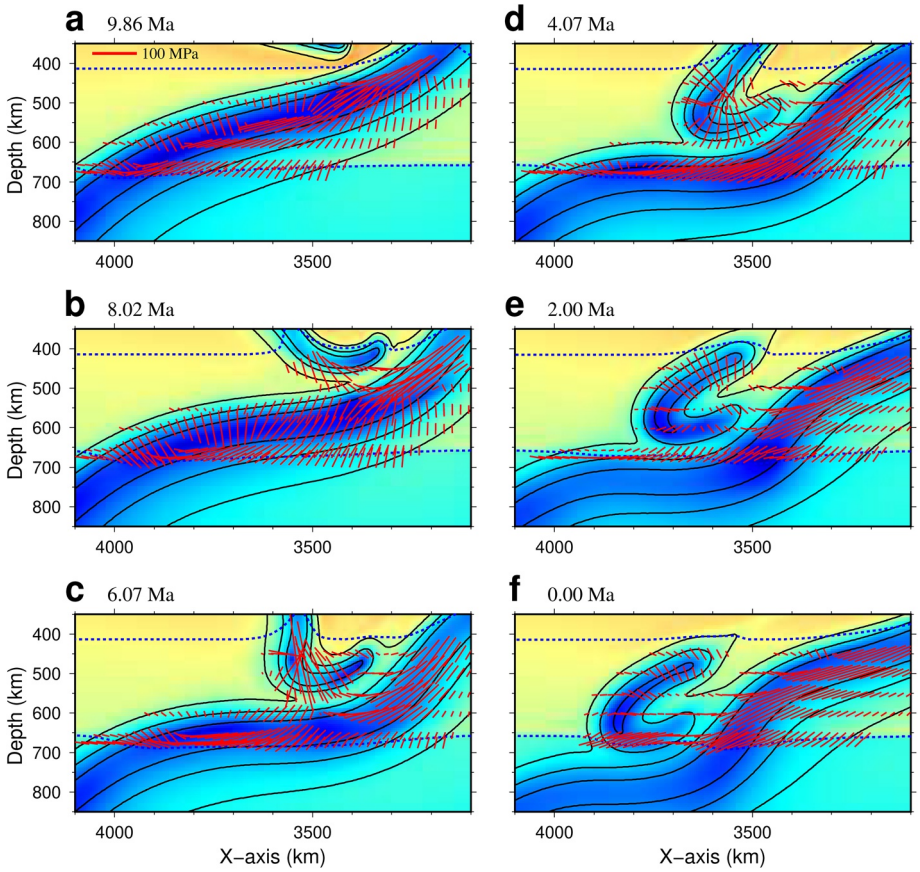

Figure 3. Evolutions of the principal compressional stress (red bars) in the transition zone during the collision between the relic and Tonga slabs (Case 1_r1). The background is viscosity, see Figure 2 for scale.

(Figure 4). Alternatively, if fully dynamic models are used, then this same kind of reversal in the state-of-stress within the upper mantle also occurs with the addition of the relic slab (Figure S12).

Based on detailed analysis of the deep earthquake doublet (Jia et al., 2020), both the *Mw* 8.2 and 7.9 ruptured mostly in the warm rim of the Tonga and relic slabs. Thus, we further explore the thermal structures of the two slabs along the overall rupture directions (purple and magenta lines in Figure S7a). The model shows that the temperature of rupture area for *Mw* 8.2 is up to 750°C if the age of the subducting Pacific plate is 100 Myr old. If we decrease the subducting plate age to 70 Myr old (with both ages being within the uncertainty of the plate reconstructions, Seton et al., 2012), the temperature increases to 810°C. In the relic slab, it is much warmer than the Tonga slab, with temperature up to 900°C–1000°C (Figure S7b). However, the computed temperature is a lower bound without heating/cooling from the exothermic phase transition at 410 km and endothermic at 660 km depth. This heating can warm the slab by ~100°C–200°C (Arredondo & Billen, 2016). Thus, we estimate temperatures of the *Mw* 8.2 and 7.9 ruptures can be at least up to ~900°C and ~1100°C, respectively. The more realistic models here verify the implications from the analyses of the earthquakes, that is local temperature likely controls the rupture details of deep earthquakes (Jia et al., 2020). Furthermore, the relic slab with a higher temperature likely makes it invisible in seismic tomography. By converting estimated slab temperature to compressional wave velocity anomaly with contributions from anharmonicity and anelasticity (Cammarano et al., 2003; Karato, 1993), a relic slab will have only a thin 1% velocity anomaly, too thin to be observed with current networks (Figure S8).

Detailed tectonic characteristics of the relic slab including its initial dip, horizontal length, detachment time, and plate age remain unclear (Table S3) and are studied with a sensitivity analysis. We test initial dip angles with 5°, 10°, and 20° (Figures S9a–S9c), small dip angles retain the stagnant Tonga slab in the

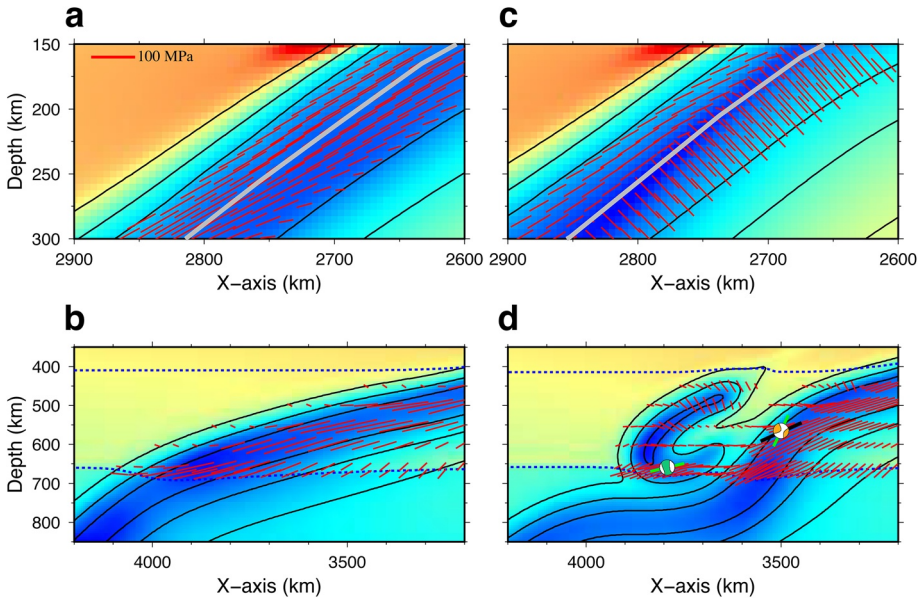

Figure 4. Stress state at shallow depth and in the transition zone (red and green rectangles in Figure 2) for Case 1 (a and b) and Case 1_r1 (c and d). The core of the slab is marked by gray line in (a and c). The 2018 Fiji deep earthquake doublet (*Mw* 8.2 and 7.9) with *P* axes orientations (green line) has been projected on the (d). The black line is the averaged orientation of *P* axes estimated from CMT solutions.

upper mantle but cannot fit tomographic images (Figures S3, S9a, and S9b). Large dip angles lead to the Tonga and relic slabs resting in the lower mantle, making seismicity at the top of the transition zone difficult to explain (Figure S9c). We vary the horizontal length of the relic slab from 600 to 500 km and 700 km (Figures S9d and S9e). These models show that deep earthquakes beneath the transition zone occur at the collision boundary, in contrast with the idea that they occur near the cold core. If the detachment time is advanced (to ~5 Ma), the short-time interaction between slabs is insufficient to produce intense deformation (Figure S9f). Increasing relic slab age (45–25 Myr) has little effect on morphology, but the compressive stress orientation is predominantly horizontal beneath the folding relic slab and inconsistent with focal mechanisms (Figure S9g). If we place relic slab closer to the transition zone, the relic slab with small-scale folding cannot explain the deep earthquakes in the entire transition zone (Figure S9h).

4. Discussion and Conclusion

Tonga slab morphology changes from more horizontal to nearly vertical in the transition zone as shown with tomographic images and seismicity; this pattern appears to be globally unique (Figure 1 and Figure S4; Conder & Wiens, 2006; van der Hilst, 1995). The elevated seismicity beneath North Fiji Basin shows a complex state-of-stress. Tonga displays a double seismic zone above 300 km depth in the northern part of the slab. In the south, the stress state becomes downdip compression throughout (Bonnardot et al., 2009; Wei et al., 2017). To explain enhanced Tonga slab deformation, mechanisms have been proposed including reactivation of preexisting faults, phase transformations, and resistance from the Pacific superplume (Gurnis et al., 2000; Jiao et al., 2000; Kirby et al., 1996). However, these mechanisms have difficulty fitting Tonga slab morphology and the complex state-of-stress. In the Tonga-relic slab model, the northern Tonga slab undergoes intense deformation in the mantle transition zone and expresses two-layered stress state close to the slab core at shallow depth which we attribute to a squeezing between the relic and Tonga slabs (Figure 4), but in the single Tonga slab model, the continuous rigid slab shows downdip compression throughout. Thus, interaction between Tonga and relic slabs in the model not only reproduces the observed high-resolution slab morphology, but also the state-of-stress estimated from focal mechanisms in the northern Tonga-Fiji subduction system. It demonstrates that variations in slab geometry play a critical role in controlling state-of-stress.

Furthermore, the excess deep earthquakes within the Tonga-Fiji subduction system are likely interpreted to be the folding and deformation due to the collision between the two slabs. The resistance imposed by the Pacific superplume may strengthen deformation (Gurnis et al., 2000). Besides, metastable olivine and postspinel phase changes would also increase the positive buoyancy and influence the state-of-stress (Kirby et al., 1996). Thus, we speculate that the well documented deep earthquakes beneath Tonga-Fiji can likely be interpreted as a consequence of intense deformation due to collision along with enhanced resistance from the Pacific plume and phase transformations.

Generally, the thermal parameter of a subduction zone has a direct relation with seismicity, a large thermal parameter associated will cause more earthquakes (Syracuse et al., 2010). However, Jia et al. (2020) proposed that local temperature controls the rupture processes of the deep earthquakes through analyses of the large doublet (*Mw* 8.2 and 7.9). We estimate the thermal structures of the Tonga and relic slabs along the rupture directions and find that the rupture areas have high temperatures of at least ~900°C and ~1100°C, verifying the implications from seismology. The thermal states of rupture areas of more large deep earthquakes in the global subduction system need to be inspected to consolidate the inference.

The geodynamic model demonstrates that impingement from a relic slab detached from the Vanuatu Trench steepens the Tonga slab and results in a folded relic slab in the mantle transition zone. This intense deformation controls the state-of-stress within these two slabs. A 3-D model with different convergence rates will be required to refine understanding of the deformation mechanism of the Tonga-Fiji subduction system.

Data Availability Statement

The mantle convection code Citcom and the *P* wave tomography models are available at https://geodynamics.org/cig/and https://www.earth.ox.ac.uk/~smachine/cgi/index.php, while model data files will be available at https://data.caltech.edu/

Acknowledgments
H. Liu's visit to Caltech was supported by the Strategic Priority Research Program of Chinese Academy of Sciences, Grant No. XDB 41000000 and the China Scholarship Council. Additional support provided by the National Science Foundation through award EAR-1645775, and National Natural Science Foundation of China (41774105 and 41820104004).

References

Alpert, L. A., Becker, T. W., & Bailey, I. W. (2010). Global slab deformation and centroid moment tensor constraints on viscosity. *Geochemistry, Geophysics, Geosystems*, *11*, Q12006. https://doi.org/10.1029/2010GC003301

Arredondo, K. M., & Billen, M. I. (2016). The effects of phase transitions and compositional layering in two-dimensional kinematic models of subduction. *Journal of Geodynamics*, *100*, 159–174. https://doi.org/10.1016/j.jog.2016.05.009

Auzende, J.-M., Lafoy, Y., & Marsset, B. (1988). Recent geodynamic evolution of the north Fiji Basin (southwest Pacific). *Geology*, *16*(10), 925–929. https://doi.org/10.1130/0091-7613(1988)016<0925:rgeotn>2.3.co;2

Barcheck, C. G., Wiens, D. A., van Keken, P. E., & Hacker, B. R. (2012). The relationship of intermediate- and deep-focus seismicity to the hydration and dehydration of subducting slabs. *Earth and Planetary Science Letters*, *349–350*, 153–160. https://doi.org/10.1016/j.epsl.2012.06.055

Billen, M. I. (2020). Deep slab seismicity limited by rate of deformation in the transition zone. *Science Advances*, *6*(22), eaaz7692. https://doi.org/10.1126/sciadv.aaz7692

Bonnardot, M. A., Régnier, M., Christova, C., Ruellan, E., & Tric, E. (2009). Seismological evidence for a slab detachment in the Tonga subduction zone. *Tectonophysics*, *464*(1–4), 84–99. https://doi.org/10.1016/j.tecto.2008.10.011

Cai, C., & Wiens, D. A. (2016). Dynamic triggering of deep earthquakes within a fossil slab. *Geophysical Research Letters*, *43*, 9492–9499. https://doi.org/10.1002/2016GL070347

Cammarano, F., Goes, S., Vacher, P., & Giardini, D. (2003). Inferring upper-mantle temperatures from seismic velocities. *Physics of the Earth and Planetary Interiors*, *138*(3–4), 197–222. https://doi.org/10.1016/s0031-9201(03)00156-0

Chen, W.-P., & Brudzinski, M. R. (2001). Evidence for a large-scale remnant of subducted lithosphere beneath Fiji. *Science*, *292*(5526), 2475–2479. https://doi.org/10.1126/science.292.5526.2475

Christensen, U. R. (1996). The influence of trench migration on slab penetration into the lower mantle. *Earth and Planetary Science Letters*, *140*(1–4), 27–39. https://doi.org/10.1016/0012-821x(96)00023-4

Conder, J. A., & Wiens, D. A. (2006). Seismic structure beneath the Tonga arc and Lau back-arc basin determined from joint Vp, Vp/Vs tomography. *Geochemistry, Geophysics, Geosystems*, *7*, Q03018. https://doi.org/10.1029/2005GC001113

Engdahl, E. R., van der Hilst, R., & Buland, R. (1998). Global teleseismic earthquake relocation with improved travel times and procedures for depth determination. *Bulletin of the Seismological Society of America*, *88*(3), 722–743.

Fan, W., Wei, S. S., Tian, D., McGuire, J. J., & Wiens, D. A. (2019). Complex and diverse rupture processes of the 2018 Mw8.2 and Mw7.9 Tonga-Fiji deep earthquakes. *Geophysical Research Letters*, *46*, 2434–2448. https://doi.org/10.1029/2018GL080997

Frohlich, C. (2006). *Deep earthquakes*. Cambridge, UK: Cambridge University Press.

Fukao, Y., & Obayashi, M. (2013). Subducted slabs stagnant above, penetrating through, and trapped below the 660 km discontinuity. *Journal of Geophysical Research: Solid Earth*, *118*, 5920–5938. https://doi.org/10.1002/2013JB010466

Green, H. W., & Houston, H. (1995). The mechanics of deep earthquakes. *Annual Review of Earth and Planetary Sciences*, *23*(1), 169–213. https://doi.org/10.1146/annurev.ea.23.050195.001125

Gurnis, M., Ritsema, J., Van Heijst, H.-J., & Zhong, S. (2000). Tonga slab deformation: The influence of a lower mantle upwelling on a slab in a young subduction zone. *Geophysical Research Letters*, *27*(16), 2373–2376. https://doi.org/10.1029/2000GL011420

Hacker, B. R., Abers, G. A., & Peacock, S. M. (2003). Subduction factory 1. Theoretical mineralogy, densities, seismic wave speeds, and H_2O contents. *Journal of Geophysical Research*, *108*(B1), 2029. https://doi.org/10.1029/2001JB001127

Hall, R., & Spakman, W. (2002). Subducted slabs beneath the eastern Indonesia-Tonga region: Insights from tomography. *Earth and Planetary Science Letters*, *201*(2), 321–336. https://doi.org/10.1016/s0012-821x(02)00705-7

Hamburger, M. W., & Isacks, B. L. (1987). Deep earthquakes in the southwest Pacific: A tectonic interpretation. *Journal of Geophysical Research*, *92*(B13), 13841–13854. https://doi.org/10.1029/JB092iB13p13841

Han, L., & Gurnis, M. (1999). How valid are dynamic models of subduction and convection when plate motions are prescribed? *Physics of the Earth and Planetary Interiors*, *110*(3–4), 235–246. https://doi.org/10.1016/s0031-9201(98)00156-3

Houston, H. (2015). *Deep earthquakes* (pp. 329–354). https://doi.org/10.1016/b978-0-444-53802-4.00079-8.287

Isacks, B., & Molnar, P. (1971). Distribution of stresses in the descending lithosphere from a global survey of focal-mechanism solutions of mantle earthquakes. *Reviews of Geophysics*, *9*(1), 103–174. https://doi.org/10.1029/RG009i001p00103

Jia, Z., Shen, Z., Zhan, Z., Li, C., Peng, Z., & Gurnis, M. (2020). The 2018 Fiji Mw 8.2 and 7.9 deep earthquakes: One doublet in two slabs. *Earth and Planetary Science Letters*, *531*, 115997. https://doi.org/10.1016/j.epsl.2019.115997

Jiao, W., Silver, P. G., Fei, Y., & Prewitt, C. T. (2000). Do intermediate- and deep-focus earthquakes occur on preexisting weak zones? An examination of the Tonga subduction zone. *Journal of Geophysical Research*, *105*(B12), 28125–28138. https://doi.org/10.1029/2000JB900314

Karato, S.-I. (1993). Importance of anelasticity in the interpretation of seismic tomography. *Geophysical Research Letters*, *20*(15), 1623–1626. https://doi.org/10.1029/93GL01767

Karato, S. I., Riedel, M. R., & Yuen, D. A. (2001). Rheological structure and deformation of subducted slabs in the mantle transition zone: Implications for mantle circulation and deep earthquakes. *Physics of the Earth and Planetary Interiors*, *127*(1–4), 83–108. https://doi.org/10.1016/s0031-9201(01)00223-0

Kirby, S. H., Stein, S., Okal, E. A., & Rubie, D. C. (1996). Metastable mantle phase transformations and deep earthquakes in subducting oceanic lithosphere. *Reviews of Geophysics*, *34*(2), 261–306. https://doi.org/10.1029/96RG01050

Macfarlane, A., Carney, J. N., Crawford, A. J., & Greene, H. G. (1988). Vanuatu—A review of the onshore geology. In H. G. Greene, & F. L. Wong (Eds.), *Geology and offshore resources of Pacific island arcs—Vanuatu region, Circum-Pacific Council for Energy and Mineral Resources Earth Science Series* (pp. 45–91). Houston, TX: Circum-Pacific Council for Energy and Mineral Resources.

Meffre, S., Falloon, T. J., Crawford, T. J., Hoernle, K., Hauff, F., Duncan, R. A., et al. (2012). Basalts erupted along the Tongan fore arc during subduction initiation: Evidence from geochronology of dredged rocks from the Tonga fore arc and trench. *Geochemistry, Geophysics, Geosystems*, *13*, Q12003. https://doi.org/10.1029/2012GC004335

Müller, R. D., Seton, M., Zahirovic, S., Williams, S. E., Matthews, K. J., Wright, N. M., et al. (2016). Ocean basin evolution and global-scale plate reorganization events since Pangea breakup. *Annual Review of Earth and Planetary Sciences*, *44*, 107–138. https://doi.org/10.1146/annurev-earth-060115-012211

Ogawa, M. (1987). Shear instability in a viscoelastic material as the cause of deep focus earthquakes. *Journal of Geophysical Research*, *92*(B13), 13801–13810. https://doi.org/10.1029/JB092iB13p13801

Ohuchi, T., Lei, X., Ohfuji, H., Higo, Y., Tange, Y., Sakai, T., et al. (2017). Intermediate-depth earthquakes linked to localized heating in dunite and harzburgite. *Nature Geoscience*, *10*(10), 771–776. https://doi.org/10.1038/ngeo3011

Pelletier, B., Lafoy, Y., & Missegue, F. (1993). Morphostructure and magnetic fabric of the northwestern North Fiji Basin. *Geophysical Research Letters*, *20*(12), 1151–1154. https://doi.org/10.1029/93GL01240

Richards, S., Holm, R., & Barber, G. (2011). When slabs collide: A tectonic assessment of deep earthquakes in the Tonga-Vanuatu region. *Geology*, *39*(8), 787–790. https://doi.org/10.1130/g31937.1

Seton, M., Müller, R. D., Zahirovic, S., Gaina, C., Torsvik, T., Shephard, G., et al. (2012). Global continental and ocean basin reconstructions since 200 Ma. *Earth-Science Reviews*, *113*(3–4), 212–270. https://doi.org/10.1016/j.earscirev.2012.03.002

Shen, Z., & Zhan, Z. (2020). Metastable olivine wedge beneath the Japan Sea imaged by seismic interferometry. *Geophysical Research Letters*, *47*, e2019GL085665. https://doi.org/10.1029/2019GL085665

Silver, P. G., Beck, S. L., Wallace, T. C., Meade, C., Myers, S. C., James, D. E., & Kuehnel, R. (1995). Rupture characteristics of the deep Bolivian earthquake of 9 June 1994 and the mechanism of deep-focus earthquakes. *Science*, *268*(5207), 69–73. https://doi.org/10.1126/science.268.5207.69

Sutherland, R., Collot, J., Bache, F., Henrys, S., Barker, D., Browne, G. H., et al. (2017). Widespread compression associated with Eocene Tonga-Kermadec subduction initiation. *Geology*, *45*(4), 355–358. https://doi.org/10.1130/g38617.1

Sutherland, R., Dickens, G. R., Blum, P., Agnini, C., Alegret, L., Asatryan, G., et al. (2020). Continental-scale geographic change across Zealandia during Paleogene subduction initiation. *Geology*, *48*(5), 419–424. https://doi.org/10.1130/g47008.1

Syracuse, E. M., van Keken, P. E., & Abers, G. A. (2010). The global range of subduction zone thermal models. *Physics of the Earth and Planetary Interiors*, *183*(1–2), 73–90. https://doi.org/10.1016/j.pepi.2010.02.004

Torsvik, T. H., Steinberger, B., Shephard, G. E., Doubrovine, P. V., Gaina, C., & Domeier, M. (2019). Pacific-panthalassic reconstructions: Overview, errata and the way forward. *Geochemistry, Geophysics, Geosystems*, *20*, 3659–3689. https://doi.org/10.1029/2019GC008402

van der Hilst, R. (1995). Complex morphology of subducted lithosphere in the mantle beneath the Tonga trench. *Nature*, *374*(6518), 154–157. https://doi.org/10.1038/374154a0

Wei, S. S., Wiens, D. A., van Keken, P. E., & Cai, C. (2017). Slab temperature controls on the Tonga double seismic zone and slab mantle dehydration. *Science Advances*, *3*(1), e1601755. https://doi.org/10.1126/sciadv.1601755

Wiens, D. A., McGuire, J. J., & Shore, P. J. (1993). Evidence for transformational faulting from a deep double seismic zone in Tonga. *Nature*, *364*(6440), 790–793. https://doi.org/10.1038/364790a0

Yang, T., Gurnis, M., & Zhan, Z. (2017). Trench motion-controlled slab morphology and stress variations: Implications for the isolated 2015 Bonin Islands deep earthquake. *Geophysical Research Letters*, *44*, 6641–6650. https://doi.org/10.1002/2017GL073989

Zhan, Z. (2020). Mechanisms and implications of deep earthquakes. *Annual Review of Earth and Planetary Sciences*, *48*. https://doi.org/10.1146/annurev-earth-053018-060314

References From the Supporting Information

Amaru, M. L. (2007). *Global travel time tomography with 3-D reference models* (Vol. 274). Utrecht, Netherlands: Utrecht University.

Bower, D. J., Gurnis, M., & Flament, N. (2015). Assimilating lithosphere and slab history in 4-D Earth models. *Physics of the Earth and Planetary Interiors*, *238*, 8–22. https://doi.org/10.1016/j.pepi.2014.10.013

Christensen, U. R., & Yuen, D. A. (1985). Layered convection induced by phase transitions. *Journal of Geophysical Research*, *90*(B12), 10291–10300. https://doi.org/10.1029/JB090iB12p10291

Čížková, H., & Bina, C. R. (2013). Effects of mantle and subduction-interface rheologies on slab stagnation and trench rollback. *Earth and Planetary Science Letters*, *379*, 95–103.

Deschamps, F., & Trampert, J. (2003). Mantle tomography and its relation to temperature and composition. *Physics of the Earth and Planetary Interiors*, *140*(4), 277–291. https://doi.org/10.1016/j.pepi.2003.09.004

Hayes, G. P., Moore, G. L., Portner, D. E., Hearne, M., Flamme, H., Furtney, M., & Smoczyk, G. M. (2018). Slab2: A comprehensive subduction zone geometry model. *Science*, *362*(6410), 58–61. https://doi.org/10.1126/science.aat4723

Holt, A. F., Becker, T. W., & Buffett, B. A. (2015). Trench migration and overriding plate stress in dynamic subduction models. *Geophysical Journal International*, *201*(1), 172–192. https://doi.org/10.1093/gji/ggv011

Hosseini, K., Sigloch, K., Tsekhmistrenko, M., Zaheri, A., Nissen-Meyer, T., & Igel, H. (2020). Global mantle structure from multifrequency tomography using P, PP and P-diffracted waves. *Geophysical Journal International*, *220*(1), 96–141. https://doi.org/10.1093/gji/ggz394

Li, C., van der Hilst, R. D., Engdahl, E. R., & Burdick, S. (2008). A new global model for P wave speed variations in Earth's mantle. *Geochemistry, Geophysics, Geosystems*, *9*, Q05018. https://doi.org/10.1029/2007GC001806

Liu, H., & Leng, W. (2020). Tarim large igneous province caused by a wide and wet mantle plume. *Journal of Geophysical Research: Solid Earth*, *125*, e2019JB019001. https://doi.org/10.1029/2019JB019001

Liu, H., Wang, W., Jia, X., Leng, W., Wu, Z., & Sun, D. (2018). The combined effects of post-spinel and post-garnet phase transitions on mantle plume dynamics. *Earth and Planetary Science Letters*, *496*, 80–88. https://doi.org/10.1016/j.epsl.2018.05.031

Lu, C., Grand, S. P., Lai, H., & Garnero, E. J. (2019). TX2019slab: A new P and S tomography model incorporating subducting slabs. *Journal of Geophysical Research: Solid Earth*, *124*, 11549–11567. https://doi.org/10.1029/2019JB017448

McNamara, A. K., Karato, S. I., & Van Keken, P. E. (2001). Localization of dislocation creep in the lower mantle: Implications for the origin of seismic anisotropy. *Earth and Planetary Science Letters*, *191*(1–2), 85–99. https://doi.org/10.1016/s0012-821x(01)00405-8

Moresi, L., Zhong, S., & Gurnis, M. (1996). The accuracy of finite element solutions of Stokes's flow with strongly varying viscosity. *Physics of the Earth and Planetary Interiors*, *97*, 83–94. https://doi.org/10.1016/0031-9201(96)03163-9

Simmons, N. A., Forte, A. M., Boschi, L., & Grand, S. P. (2010). GyPSuM: A joint tomographic model of mantle density and seismic wave speeds. *Journal of Geophysical Research*, *115*, B12310. https://doi.org/10.1029/2010JB007631

Turcotte, D., & Schubert, G. (2014). *Geodynamics*. Cambridge, UK: Cambridge University Press.

Yang, T., Gurnis, M., & Zahirovic, S. (2018). Slab avalanche-induced tectonics in self-consistent dynamic models. *Tectonophysics*, *746*, 251–265. https://doi.org/10.1016/j.tecto.2016.12.007

Zhong, S. (2006). Constraints on thermochemical convection of the mantle from plume heat flux, plume excess temperature, and upper mantle temperature. *Journal of Geophysical Research*, *111*, B04409. https://doi.org/10.1029/2005JB003972

Zhong, S., & Gurnis, M. (1995). Mantle convection with plates and mobile, faulted plate margins. *Science*, *267*(5199), 838–843. https://doi.org/10.1126/science.267.5199.838